

Machine learning surrogates for molecular dynamics simulations of soft materials

JCS Kadupitiya^a, Fanbo Sun^a, Geoffrey Fox^a and Vikram Jadhao^{a,*}

^aIntelligent Systems Engineering, Indiana University, Bloomington, Indiana 47408

ARTICLE INFO

Keywords:

Machine Learning
Molecular Dynamics Simulations
Parallel Computing
Scientific Computing
Soft Materials

ABSTRACT

Molecular dynamics (MD) simulations accelerated by high-performance computing (HPC) methods are powerful tools to investigate and extract the microscopic mechanisms characterizing the properties of soft materials such as self-assembled nanoparticles, virus capsids, confined electrolytes, and polymeric fluids. In this paper, we extend the idea developed in our earlier work of integrating machine learning (ML) methods with HPC-accelerated MD simulations of soft materials in order to enhance their predictive power and advance their applications for research and educational activities. Parallelized MD simulations of self-assembling ions in nanoconfinement are employed to demonstrate our approach. We find that an artificial neural network-based regression model successfully learns nearly all the interesting features associated with the output ionic density profiles over a broad range of ionic system parameters. The ML model generates predictions that are in excellent agreement with the results from MD simulations. The inference time associated with the ML model is over a factor of 10,000 smaller than the corresponding parallel MD simulation time. Through this demonstration, we introduce a “machine learning surrogate” for MD simulations of soft-matter systems. We develop and deploy a web application on nanoHUB to realize the advantages associated with the ML surrogate. The results demonstrate that the performance of MD simulations can be further enhanced by using ML, enabling rapid and accurate simulation-driven exploration of soft material design space.

1. Introduction

Molecular dynamics simulations are powerful tools for investigating the microscopic origins of the behavior of materials including soft matter. These simulations have enabled the understanding of microscopic mechanisms underlying the assembly of both biological and synthetic soft materials such as virus capsids [47, 20], confined electrolytes [3], polymeric liquids [40, 26], and self-assembled nanostructures [18, 10]. The molecular dynamics (MD) method solves Newton’s equation of motion for a system of many particles and evolves the positions, velocities, and forces associated with these particles at each time step. While MD simulations are generalizable to study a broad range of phenomena in soft matter, they incur high computational costs in several applications where the computational complexity per time step is proportional to the square of the total number of particles.


The high computational costs associated with MD simulations are typically mitigated by employing high-performance computing (HPC) resources and utilizing parallel computing techniques such as OpenMP and MPI. For example, in a typical MD simulation of electrolyte ions confined by material surfaces [3, 32, 37], ≈ 1 nanosecond of dynamics of ≈ 500 ions on one processor takes ≈ 12 hours of runtime. This timescale is prohibitively large to extract converged results for ion distributions that generally require ≈ 5 nanoseconds of simulated dynamics. Performing the same simulation on a single node with 16 cores using OpenMP shared memory reduces the runtime by a factor of 10 (≈ 1 hour), enabling sim-

ulations of the same system for longer physical times. Using MPI dramatically enhances the simulation performance: for systems with thousands of ions, speedup of over 100 can be achieved with 8 nodes and 16 cores per node, enabling the generation of the needed data for evaluating converged ionic distributions over a broad region of parameters characterizing the ionic system design space. Further, a hybrid OpenMP/MPI approach can provide an even higher speedup of over 400 for systems of similar number of ions with 32 nodes and 16 cores per node, enabling MD simulations that can explore the long-time dynamics of a large number of ions with fewer controlled approximations [35].

In addition to enabling innovative research, the HPC-accelerated MD simulations are useful educational tools for teaching materials science and engineering courses [23]. However, despite the employment of the optimal parallelization models suited for the size and complexity of the system, simulations can often take hours or days to furnish accurate output data and desired information. To expedite MD simulation-driven design of advanced soft materials, it is desirable to rapidly access trends associated with relevant physical quantities that could be learned and predicted with reasonable accuracy based on the history of data generated from earlier simulation runs. Further, in the area of using simulations in education, rapid access to simulation-driven responses to student questions in classroom settings are desirable. In the end, there is a critical need for new approaches to accelerate simulations, leverage past simulations to generate accurate predictions, and expedite the analysis of simulation data to classify material properties.

Machine learning (ML) has the potential to address this critical need directly. Accordingly, there has been a surge in the use of ML to accelerate computational techniques aimed

*Corresponding author

 vjadhao@iu.edu (V. Jadhao)

ORCID(s): 0000-0002-8034-2654 (V. Jadhao)

at understanding material phenomena [16]. ML has been used to predict parameters, generate configurations in material simulations, and classify material properties [52, 49, 42, 45, 13, 5, 7, 43, 16, 19, 35]. Motivated by the advancements in ML and by the challenges in employing MD simulations in research and education, in a recent paper [36], we introduced the idea of integrating ML methods with MD simulations to enhance their performance and overall usability. We demonstrated that an artificial neural network (ANN) based regression model, trained on data generated via MD simulations, successfully learns a small number of pre-identified features associated with the simulation output. The ML model instantaneously generated predictions in excellent agreement with results obtained from explicit MD simulations [36].

In this paper, we extend the original idea to solve the problem of capturing nearly all the interesting features of the desired simulation output. We utilize the MD simulations of ions in nanoconfinement employed in our earlier work [32, 36] to demonstrate the extension of the idea. While the earlier paper showed a relatively small number (3) of ML-generated predictions for the ionic distribution, we now demonstrate that the ANN model trained on the same dataset yields accurate predictions for ≈ 150 output parameters, enabling the estimation of almost all the interesting features of the ionic density profile for a wide range of system parameters. The inference time associated with the ML method is over a factor of 10,000 smaller than the corresponding MD simulation time. Through this demonstration, we introduce a first-of-its-kind “machine learning surrogate” for MD simulations of soft-matter systems.

These ML surrogates for MD simulations expand the research explorations to a much broader set of model parameters, enabling the rapid identification of interesting regimes and reliable estimates of soft material properties. In addition to expediting research, real-time access to simulation-driven responses to student questions enables a dynamic environment for using simulation for educational activities in classroom settings. To realize these advantages, we integrated the ML surrogate with a web application on nanoHUB: Ions in nanoconfinement. The ML-enhanced GUI delivers a dynamic and responsive environment to users, providing instantaneous and accurate predictions of the ionic density profile over a wide range of ionic attributes.

The organization of the paper is as follows. Sec. 2 provides the background and related work. Sec. 3 describes the ML surrogate approach. Sec. 4 presents the results of the application of the ML surrogate to the example soft-matter framework of self-assembling ions in nanoconfinement. Finally, Sec. 5 provides a brief discussion and summary including our plans for future work. For the sake of clarity and continuity, we review some important findings from the original conference paper [36] as preliminary results in Sec. 4. Similarly, some of the content in the background and related work in the original paper is repeated here.

2. Background and Related Work

MD simulations serve as essential tools for understanding diverse self-assembly phenomena in nanoscale materials [27, 30, 18], predicting material behavior in practical applications [25], and isolating interesting regions of parameter space for experimental exploration [9]. As in our original conference proceedings [36], we focus specifically on MD simulations of ions in nanoconfinement in this work to illustrate the idea of ML surrogates.

2.1. MD simulations of ions in nanoconfinement

Electrolyte ions drive key processes involved in the generation and function of soft materials such as the morphological changes in proteins, stabilization of colloids, pattern formation in nanostructures, and emulsion-based extraction of metal ions from wastewater. As a result, investigating the self-assembly of ions and extracting their distributions in nanoconfinement created by surfaces of materials such as nanoparticles, colloids, or biological macromolecules has been the focus of many experimental, theoretical, and computational studies [44, 4, 27, 29, 51, 28, 46, 15]. Confined electrolyte solutions themselves are important soft-matter systems that are ubiquitous in biology and modern technological devices such as supercapacitors [3, 44, 2, 50, 32].

From a computational modeling standpoint, the ions are represented as spheres of finite size, the material surfaces are often treated as planar interfaces considering the size difference between the ions and the confining material particles, and the solvent is coarse-grained to speed-up the simulations. Such coarse-grained MD simulations have been employed to extract the ionic distributions over a wide range of electrolyte concentrations, ion valencies, and interfacial separations using codes developed in individual research groups [3, 6, 32] or using general purpose software packages such as ESPRESSO [41] and LAMMPS [48].

2.2. ML-enhanced simulations of materials

Recent years have seen a surge in the use of ML to accelerate computational techniques aimed at understanding material phenomena. ML has been used to predict parameters, generate configurations in material simulations, design coarse-grained potentials, and classify material properties [7, 16, 42, 52, 53, 22]. For example, Fu et al. [42] employed ANN to select efficient updates to accelerate Monte Carlo simulations of classical Ising spin models near the phase transition. Botu et al. [7] employed kernel ridge regression to accelerate MD method for nuclei-electron systems by learning the selection of probable configurations in MD simulations, which enabled bypassing explicit simulations for several steps. More recently, ML has been used to predict specific outcomes (the dissociation timescale of compounds) of *ab initio* MD simulations by bypassing the time evolution of the particle trajectories [22]. Also, convolutional neural network based ML “emulators” have been introduced recently to predict output functions (e.g., power spectrum) of simulations in biogeochemistry and other domains [38]. However, relative to “hard” condensed matter systems, a sur-

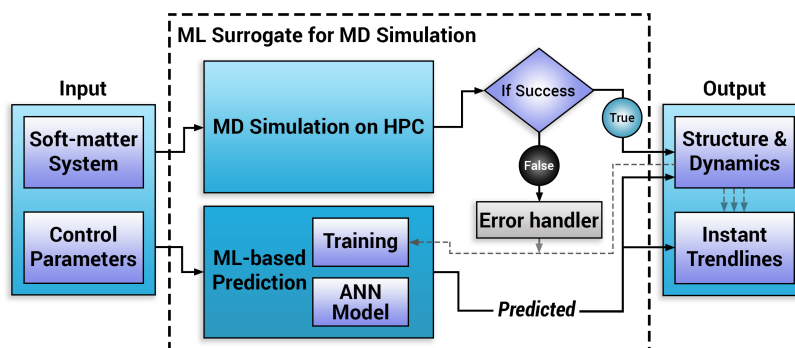


Figure 1: System overview of the ML surrogate for MD simulation approach for generating rapid and accurate predictions associated with soft material behavior.

vey of literature finds far fewer applications of ML in the area of MD simulations of soft materials [16, 35].

2.3. ML-enhanced simulations as web applications

nanoHUB is the largest online resource for education and research in nanotechnology [39]. This cyberinfrastructure hosts over 500 web applications for launching simulations and serves 1.4 million users worldwide. nanoHUB provides online access for executing simulation codes to researchers, students, and educators. We have deployed MD simulation frameworks as computational tools on nanoHUB to explore diverse self-assembly phenomena in materials. These tools are: Ions in Nanoconfinement [37], Nanosphere Electrostatics Lab [34], Nanoparticle Assembly Lab [8], and Polyvalent Nanoparticle Binding Simulator. The “Ions in nanoconfinement” tool [37] has been extensively employed by students to learn nanoscale self-assembly concepts [23]. In about 2 years since its launch, this nanoHUB tool has been used by over 100 users and run over 2600 times [37].

The integration of ML for performance enhancement of scientific simulation frameworks deployed as web applications is relatively far less explored. Our survey indicated that only one simulation tool on nanoHUB [21] employs ML-based methods to enhance the performance and usability of the simulation software. This simulation tool employs a deep neural network to bypass computational limitations in extracting transfer times associated with the excitation energy transport in light-harvesting systems [21].

3. ML Surrogates for MD Simulations

We now describe a general approach, first introduced in Ref. [36], that utilizes ML to enhance MD simulations, significantly improving their use in research and education. The “ML surrogates for MD simulations” framework can be broadly defined as the approach where an ML model, trained on data from completed simulations, is used to approximate the complex relationships between the physical input parameters and the output functions of simulations, bypassing the explicit computation of the trajectory evolution of the simulated components. Figure 1 shows the overview of this framework in the context of soft materials engineering

applications to predict the structural and dynamical properties (outputs) of the soft-matter system over a broad range of experimental control parameters (inputs). First, the attributes of the soft-matter system and the control parameters are fed to the framework (Figure 1). These inputs are used to launch the MD simulation on the HPC cluster. Simultaneously, these inputs are fed to the ML-based prediction module. Both the MD and ML methods are designed to extract (predict) the desired output quantities. Error handler aborts the MD simulation program and displays appropriate error messages when a simulation fails due to any pre-defined criteria. At the end of the simulation run, the output quantities are saved for future retraining of the ML model, which occurs after a set number of new successful simulation runs. After yielding a sufficiently large set of predictions, the ML surrogate rapidly provides trendlines capturing the behavior of output quantities as a function of variation in input parameters.

ML surrogates for MD simulations enable several capabilities: (i) learn pre-identified interesting features associated with the simulation outputs, (ii) generate accurate predictions for unseen state points, (iii) enable instantaneous predictions, and (iv) improve interactivity with anytime access to simulation results.

We now describe the application of this framework to the specific case of MD simulations of ions in nanoconfinement to illustrate the approach in further detail. Here, the goal is to extract the distribution of ions confined by two material surfaces represented as identical, uncharged parallel plates at $z = -h/2$ and $z = h/2$ (creating a confinement length of h). The inputs include the attributes of the electrolyte ions such as valency and size, and the control parameters such as electrolyte concentration and interface separation. The outputs include the density profiles or distribution functions of ions in confinement. These parameter choices enable a rich competition between electrostatic and steric forces characterizing the ionic dynamics and structure in nanoconfinement.

Our earlier work [36] showed that an artificial neural network (ANN) model can accurately predict 3 key output features: contact density, peak density, and mid-point density of confined ions. ANN outperformed other ML techniques such as polynomial regression, support vector regression,

decision tree regression, and random forest regression. In this paper, we show that the ANN model can generate predictions for nearly all the desired features of the ionic density profile, producing almost the entire ionic distribution in excellent agreement with explicit MD simulation results.

3.1. Data Generation, Preparation, and Preprocessing

Prior domain experience and backward elimination using the adjusted R squared is used for selecting the most significant input parameters for creating the training data set. This process determines which inputs are important to change the desired output. The process begins with all possible inputs and eliminates them one by one, monitoring the adjusted R squared value to determine which are important. Dropping of an input that produces a sharp spike in the R squared value is indicative of the high importance of the input parameter. Using this process, five input parameters characterizing the ionic system are identified: confinement length h , salt (electrolyte) concentration c , positive ion valency z_p , negative ion valency z_n , and the ion diameter d . All ions are assumed to have the same diameter; in general, oppositely charged ions have different sizes. The range of each parameter is selected as follows: $h \in (3.0, 4.0)$ nm, $c \in (0.3, 0.9)$ M, $z_p \in 1, 2, 3$, $z_n \in -1$, and $d \in (0.5, 0.75)$ nm. The salt concentration is defined as the number of negative ions per unit volume [36, 35, 32]. We note that system temperature is another important input parameter. In this initial application, temperature is held fixed and we have employed data generated at room temperature (298 K). Min-max normalization filter is applied to normalize the input data at the preprocessing stage.

The converged distribution for positive ions is selected as the output. The dataset created for investigations in the earlier work [36] is reused. This dataset was generated by sweeping over a few discrete values for each of the input and output parameters to create and run 6,864 MD simulations utilizing HPC resources. On average, each MD simulation was performed in the NVT (canonical) ensemble for over ≈ 5 nanoseconds of ionic dynamics, and took 4200 CPU hours (≈ 36 minutes per simulation with MPI/OpenMP parallelization). The training dataset creation took approximately 25 days including the queue wait times on the Indiana University BigRed2 supercomputing cluster. The data associated with the ionic density profiles (dataset relevant to our investigation), was over 2 GB.

The entire data set is separated into training and testing sets using a ratio of 0.8:0.2. In our earlier work, contact density ρ_c , mid-point (center of the slit) density ρ_m , and peak density ρ_p associated with the final (converged) distribution for positive ions were selected as the output parameters [36]. Each MD simulation produces positive ion distribution characterized by ionic density measured at ≈ 300 positions as output. For simplicity, using the symmetry of ionic density around the confinement center $z = 0$ (resulting from neutral surfaces), approximately half of the 300 points are selected as the output parameters to train the ML surrogate.

Accordingly, in the experiments that follow, ML is employed to make $P \approx 150$ predictions characterizing the density of ions in the left half of the confinement (with $z \in (-h/2, 0)$).

3.2. Feature Extraction and Regression

Following earlier paper [36], the ANN architecture with 2 hidden layers (Figure 2) is implemented in TensorFlow [1] for regression and prediction of $P \approx 150$ continuous (output) variables. The process of regression first determines weights and biases in the two hidden layers following an error backpropagation algorithm, implemented via a stochastic gradient descent procedure. This process employs an iterative learning algorithm that uses a training dataset to update the weights and biases in the hidden layers. Regression is done by a simple forward prediction.

The size of the hidden layers was chosen to be over 150 informed by the higher dimensions of the output data. By performing a grid search, hyper-parameters such as the number of first hidden layer units, second hidden layer units, batch size, and the number of epochs are optimized to 512, 256, 25, and 4000 respectively. The batch size is a hyper-parameter of the stochastic gradient descent algorithm that controls the number of training samples that are allowed to pass through the model before its internal parameters are updated. The number of epochs is a hyperparameter that controls the number of complete passes made through the entire training dataset. Adam optimizer is used to optimize the error backpropagation. The learning rate of Adam optimizer and the dropout rate in the dropout layer is set to 0.0001 and 0.15 respectively to prevent overfitting. Both learning and dropout rates were selected using a trial-and-error process.

The weights in the hidden layers and in the output layer are initialized for better convergence using a Xavier normal distribution at the beginning. Xavier normal distribution is characterized with 0 mean and $\sigma = 1/(\sqrt{h_i + h_o})$ variance, where h_i and h_o are input and output sizes of the hidden layers, respectively [17]. The L2 error (mean square loss) between target and predicted ionic density values is used for error calculation. ANN implementation, training, and testing are programmed using scikit-learn, Keras, and TensorFlow ML libraries [14, 11, 1]. Scikit-learn is used for grid search and scaling, Keras is used to save and load models, and TensorFlow is used to create and train the neural network.

4. Results

4.1. Preliminary Results

In our earlier work [36] we experimented with 6 regression models to predict the key output density features identified above: contact density (ρ_c), mid-point density (ρ_m), and peak density (ρ_p). These models were tested on 2060 sets of input parameters (h, z_p, z_n, c, d). Table 1 shows the success rate and the mean square error (MSE) for testing data sets. The success rate was calculated based on the error bars associated with the density values obtained via MD simulations: ML prediction was considered successful when the predicted density value was within the error bar of the simulation estimate. Simulations were run for sufficiently long times (over

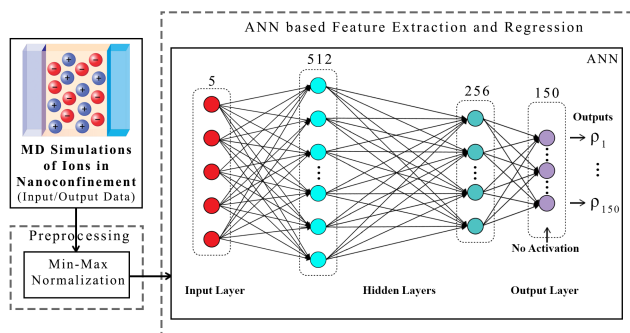


Figure 2: Artificial neural network based regression model used in the ML surrogate to predict output ionic density profile of ions in nanoconfinement.

≈ 5 nanoseconds) to obtain converged density estimates and error bars. MSE values are calculated using k -fold cross-validation techniques with $k = 20$. k -fold cross-validation is a statistical technique commonly used in applied ML to estimate the accuracy of the ML models. This approach involves randomly dividing the set of observations into k groups, or folds, of approximately equal size. The first fold is treated as a validation set, and the method is fit on the remaining $k - 1$ folds. The test accuracy is determined by taking the average over $(k - 1)$ folds.

ANN-based regression model with implementation details described in Sec. 3 predicted ρ_c , ρ_m and ρ_p accurately with a success rate of 95.52%, 92.07%, and 94.78% respectively. MSE values for each of these predictions were small as shown in Table 1. ANN outperformed all other non-linear regression models investigated (Table 1) including Polynomial, Kernel-Ridge, Support Vector, Decision Tree and Random Forest. Among these other models, the highest average success rates of 80.11%, 79.55%, and 81.89% for predictions of ρ_c , ρ_m and ρ_p values respectively were obtained for the Support Vector regression model [36]. To enable a clear comparison of ANN results with those obtained via other regression models, we discuss briefly the implementation details associated with other methods below.

Polynomial regression was tested with scikit-learn “PolynomialFeatures”. Different “degree” parameter values (representing the order of the polynomial used to approximate the target function) were experimented with and the highest reported accuracy was obtained for degree of 4. Support Vector was tested with scikit-learn “SVR” implementation and we experimented with different kernel transformation functions such as linear, polynomial, radial basis function (rbf), and sigmoid. The highest reported accuracy was obtained for the rbf kernel with kernel coefficient $\gamma = 0.1$, and the following optimization (meta) parameters: regularization parameter $C = 100$, and no-penalty distance $\epsilon = 0.1$. Kernel-Ridge model was tested with scikit-learn “Kernel ridge regression (KRR)” implementation. Experiments with different input arguments for the kernel transformation function were performed; the highest reported accuracy was obtained for the rbf kernel with kernel coefficient $\gamma = 0.1$.

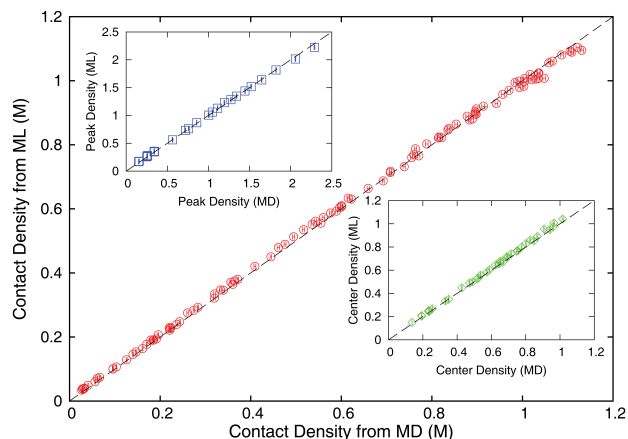


Figure 3: Accuracy comparison between ML predictions and MD simulation results for the contact densities (red circles) of ions in systems characterized by inputs selected from the following ranges of parameters: $h \in (3.0, 4.0)$ nm, $z_p \in 1, 2, 3$, $z_n \in -1, -2$, $c \in (0.3, 0.9)$ M, and $d \in (0.5, 0.75)$ nm. Top-left and bottom-right insets show the comparison for the peak (blue squares) and mid-point (green diamonds) densities respectively for a subset of the selected systems. Black dashed lines with a slope of 1 represent perfect correlation. All densities are shown in units of molar.

Decision Tree was tested with scikit-learn “DecisionTreeRegressor” implementation and we experimented with different input arguments for the maximum depth of the tree and the highest reported accuracy was obtained for the maximum depth of 4. Random Forest was tested with scikit-learn “RandomForestRegressor” implementation and we experimented with different input arguments for maximum depth of the tree and the number of trees in the forest. The highest reported accuracy was obtained for maximum depth of 4 and 25 number of trees. All these methods as well as the ANN model were trained and validated with the same test data.

Figure 3 shows the comparison between the predictions made by the ML model and the results obtained from MD simulations for the contact, mid-point, and peak densities associated with positive ions [36]. Results are shown for a randomly selected subset of the entire testing dataset described in Section 3.1. ρ_c , ρ_m and ρ_p predicted by the ML model were found to be in excellent agreement with those calculated using the MD method; data from either approach fall on the dashed lines which indicate perfect correlation.

4.2. ML surrogate accuracy and validation

We now describe the extension of the ANN model to make accurate predictions over a much larger set of output ionic density values. In order to demonstrate this, we examine both the overfitting characteristics and the accuracy of the model. Overfitting characteristics are assessed by comparing two losses: training loss on training data and validation loss on test data. Training loss is the average of the MSE between the prediction and the target values for all training data. Validation loss is the average of the MSE between the prediction and the target values for all testing data. The train-

Table 1

Comparison of regression models for the prediction of output ionic density values.

Model	Contact Density		Midpoint Density		Peak Density	
	Success %	MSE	Success %	MSE	Success %	MSE
Polynomial	61.04	0.0129300	60.84	0.0187700	61.87	0.0100400
Kernel-Ridge	78.86	0.0030900	76.57	0.0041200	75.93	0.0049800
Support Vector	80.11	0.0012700	79.55	0.0024900	81.98	0.0010600
Decision Tree	68.44	0.0084600	64.54	0.0094900	62.47	0.0110700
Random Forest	74.15	0.0045700	70.85	0.0078900	75.09	0.0040800
ANN-based	95.52	0.0000718	92.07	0.0002293	94.78	0.0002306

ing and validation loss on 5491 and 1373 simulations decrease to 0.000194 and 0.000024 respectively within 4000 epochs of training. Similar amounts of reduction in training and validation losses indicates that the ML model is not overfitted [12].

Typically, in regression problems, accuracy or success rate is inherently not defined. To facilitate the comparison of ML predictions with MD results, we define a prediction as successful when the density value predicted by the ML surrogate ρ^{ML} is within the error ϵ associated with the corresponding MD simulation estimate ρ^{MD} (ground truth). For each simulation, the MD result for the output ionic density is represented by a set of ≈ 150 points associated with the discretized positions characterizing the confinement length. The n^{th} prediction made by the ML model corresponds to the n^{th} element in this output set. We define the average success rate or accuracy associated with the ML approach for the n^{th} prediction as:

$$A_n = \frac{1}{N_{\text{test}}} \sum_{i=1}^{N_{\text{test}}} \Theta \left(\left| \rho_{n,i}^{\text{ML}} - \rho_{n,i}^{\text{MD}} \right|, \epsilon_{n,i} \right) \quad (1)$$

where i indicates the simulation index, N_{test} is the number of samples (simulations) in the test data, and $\Theta(x, \epsilon)$ is a step function given by: $\Theta(x, \epsilon) = 1$ for $x < \epsilon$, and $\Theta(x, \epsilon) = 0$ for $x \geq \epsilon$. The overall ensemble-average success rate A of the ML prediction for the entire density profile can be estimated using $A = (1/P) \sum_{n=1}^P A_n$, where the sum is now over the total number of predictions P .

Figure 4 shows the success rate A_n associated with the n^{th} ML prediction for the testing dataset. In order for the prediction to be well-evaluated, A_n is only computed for ML predictions associated with non-vanishing ρ^{MD} ($\rho^{\text{MD}} \neq 0$). In other words, results are not shown for ≈ 20 output parameters ($P \approx 130$) where the ionic density and associated error from MD simulations are exactly 0 (regions near the left wall where finite-sized ions are prohibited from entering). As Figure 4 shows, A_n is very good for all the evaluated ML predictions. The ensemble-average success rate is found to be $A = 0.958$, and the lowest and highest recorded values for accuracy are $A_n = 0.86$ and $A_n = 0.997$ respectively.

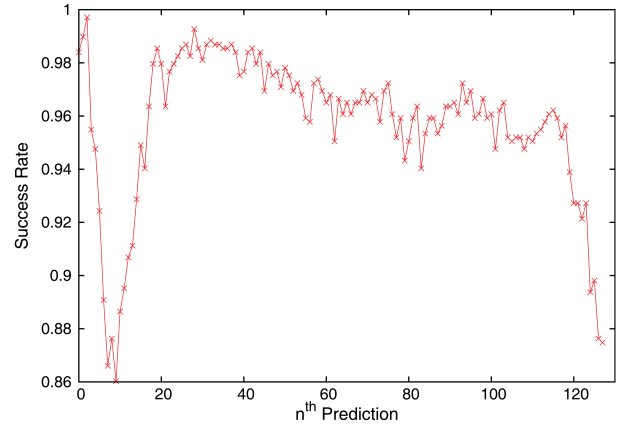


Figure 4: Success rate A_n associated with the n^{th} prediction made by the ML surrogate (A_n is defined in Eq. 1).

4.3. Ionic density profiles: comparing ML surrogate predictions and MD simulations

We now present plots of the positive ion density profiles showing the comparison between the predictions made by the ML surrogate and the results obtained from MD simulations. Results are shown for a set of 4 systems randomly selected from the entire testing dataset. These 4 systems are: system I (3.2, 1, -1, 0.6, 0.65), system II (3.6, 3, -1, 0.9, 0.75), system III (3.3, 3, -1, 0.35, 0.714), and system IV (3.6, 1, -1, 0.9, 0.6), where the parentheses list the 5 aforementioned input parameters characterizing the ionic system: confinement length h , positive ion valency z_p , negative ion valency z_n , salt concentration c , and ion diameter d . Figure 5 (a) - (d) shows the ionic density profiles predicted by the ML surrogate for systems I, II, III, and IV respectively. As the figure indicates, for each system, the ML-predicted density profile is in excellent agreement with the result extracted using MD simulation (ground truth).

To make the comparison between ML predictions and MD simulation results more quantitative, we extract the overall accuracy of the ML prediction for each system (density profile). Similar to Eq. 1, we define this accuracy or success rate A_i associated with the i^{th} system (simulation configura-

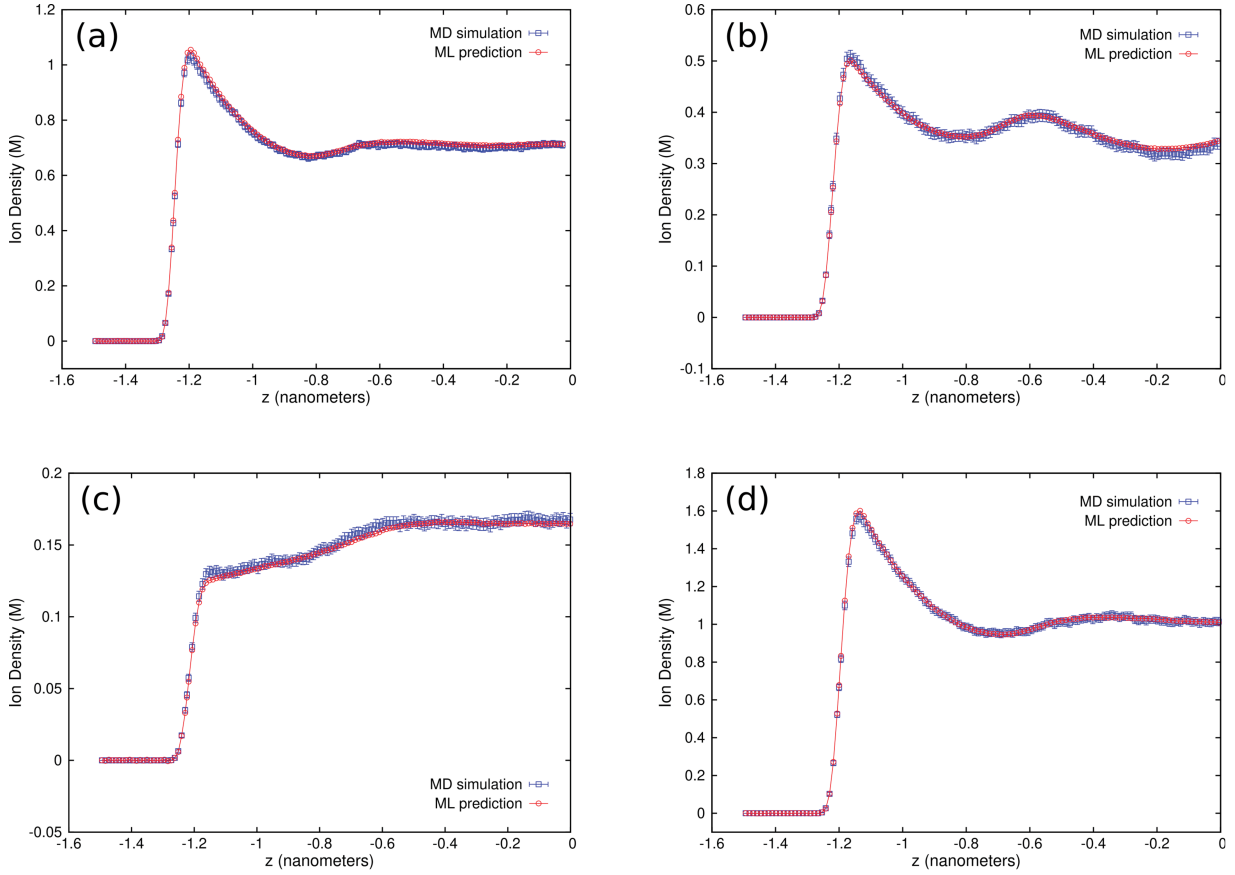


Figure 5: Ionic density profiles for systems I (a), II (b), III (c), and IV (d) predicted by the ML surrogate (red circles) and extracted with MD simulation (blue squares). See main text for system definitions.

tion) as:

$$A_i = \frac{1}{P} \sum_{n=1}^P \Theta \left(\left| \rho_{n,i}^{\text{ML}} - \rho_{n,i}^{\text{MD}} \right|, \epsilon_{n,i} \right) \quad (2)$$

where Θ is the step function defined above, and the sum is over the total number of predictions P made using the ML approach (as before, A_i is meaningful only at non-zero ionic density values, making $P \approx 130$). Using Eq. 2, the success rates A_i for systems I, II, III, and IV are found to be 0.98, 0.91, 0.78, 0.89 respectively. Success rate A_i represents the number of discrete positions (z) where the ML predictions of density values were found to be within the error bounds produced by the associated MD simulation results. For example, a success rate of 89% means that density values at 89 discrete positions out of 100 were predicted within the uncertainty obtained from MD simulations. As discussed above, compared to results obtained using other regression models which showed a maximum success rate of $\approx 80\%$ for density predictions at different positions within the confinement, ANN success rates for predicting the entire density profile are better on average. We also point out that the ML inferences are made at a relatively much smaller time of ≈ 0.2 seconds compared to MD simulations (see below for further details).

4.4. Instantaneous trendlines using ML surrogates

The good agreement between ionic densities generated via ML surrogate and MD simulations as well as the much smaller “lookup time” for obtaining the ML inferences enable the generation of trendlines for the entire density profile almost instantaneously. Figure 6 shows a selected subset of these ML-surrogate-predicted trendlines exhibiting the variation of ion distributions with changes in input parameters.

Figure 6 (a) and (b) shows the variation in the density of positive ions of valency $z_p = 1, 2, 3$ at salt concentration $c = 0.5$ M and 0.9 M respectively (note that we define $c = N_n/V$, where N_n is the number of negative ions and V is the simulated volume). Other input parameters are fixed to $h = 3.0$ nm, $z_n = -1$, and $d = 0.7$ nm. The ML-generated trendlines are able to track distinct variations in density for different ion valencies and salinity conditions. Using Eq. 2, the success rates A_i associated with ML predictions of profiles for ions of valency 1, 2, 3 at $c = 0.5$ M (Fig. 6 a) are found to be 0.93, 0.98, and 0.92 respectively. Similarly A_i values associated with ML predictions of profiles for ions of valency 1, 2, 3 at $c = 0.9$ M (Fig. 6 b) are 0.93, 0.96 and 0.89 respectively. The peak of the ionic density and the number of oscillations increase with c . Further, at a given c , increasing the ion valency leads to the depletion of ions near the left surface (reduced ion density near $z = 0$). Both these observations inferred by the ML surrogate follow the expected

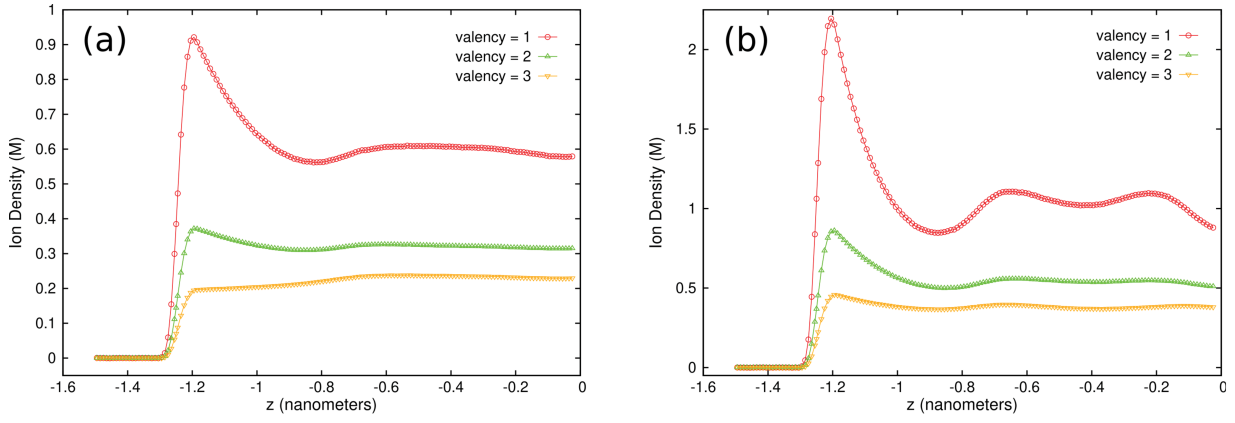


Figure 6: Trendlines generated using ML surrogate to examine variation in ionic density with positive ion valency at salt concentration (a) $c = 0.5$ M and (b) 0.9 M. See main text for values of other input system parameters.

behavior in these systems as reported and elucidated in previous work [32].

4.5. ML inference time and overall speedup

In the earlier paper [36], we introduced a simple formula illustrative of the possible gains or speedup S resulting from the use of scientific ML surrogates:

$$S = \frac{t_{sim}}{t_p + t_{tr} \cdot N_p / N_{tr}}, \quad (3)$$

where t_{sim} is the time to run the MD simulation via the sequential model, t_p is the time it takes for the ML surrogate to make a prediction (or “lookup” time) for one set of inputs, N_p is the number of ML predictions made, N_{tr} is the number of elements in the training dataset, and t_{tr} is the average walltime associated with the MD simulation to create one of these elements. $N_{tr}t_{tr}$ is the total time to create the training dataset which includes the generation of the training data using MD simulations and the TensorFlow training time.

In the specific case of the system of confined ions considered above, the training dataset consisted of 5491 simulation configurations ($N_{tr} = 5491$). The time t_{tr} to generate one element of this training set is similar to the average runtime of the parallelized MD simulation. For the MD simulations considered in this work, $t_{sim} \approx 60$ hours, $t_{tr} \approx 36$ minutes, and ML inference time $t_p \approx 0.2$ seconds. Comparing the run times of the parallelized MD simulation and the ML surrogate, we find that the ML surrogate yields output results over 10,000 ($= t_{tr}/t_p$) times faster than parallel MD simulation. We also note that the ML surrogate is using 1 core to infer the result as compared to 128 cores employed by the parallel simulation, indicating a complementary reduction in resource utilization by a factor of 128.

Given $t_p \ll t_{tr}$ and approximating $t_p \rightarrow 0$ in Eq. 3, we find $S = S_{HPC} N_p / N_{tr}$, where $S_{HPC} = t_{sim}/t_{tr}$ is the traditional speedup obtained by parallelizing the MD simulation using HPC resources. We can identify the ML-only speedup as $S_{ML} = N_p / N_{tr}$, i.e., the number of predictions made by the ML surrogate divided by the size of the training dataset. The key feature of the ML-based approach is thus

highlighted: S rises with increasing N_p , that is, the speedup increases as the ML surrogate is used to make more predictions. We also observe that for ML-enabled results to generate a “true” net speedup ($S > 1$), the number of predictions made by the surrogate (ANN model) per one forward propagation must exceed N_{tr}/S_{HPC} , that is, $N_p > N_{tr}/S_{HPC}$. For the example considered here, $S_{HPC} = 100$, yielding the relation $N_p \gtrsim 60$. Considering this inequality, the use of ML surrogate enhances the overall efficiency of the simulation framework when it predicts over 60 ionic density profiles.

4.6. ML-enhanced nanoHUB application

In our original work [33], we proposed to extend the usability of a nanoHUB computational tool, “Ions in nanoconfinement” [37], by integrating ML-based enhancements. This tool enables investigations into the self-assembly of electrolyte ions in nanoconfinement, and has been employed to teach courses in Indiana University on nanoscale simulation [23]. Our initial design focused on predicting ionic density for three positions (contact, mid-point, peak) [36]. Building on the extended ANN model, we designed the integration of the ML surrogate with the nanoHUB tool to predict almost all the interesting features of the ionic density profile (with ≈ 150 predicted density values). In October 2019, we deployed this enhanced application using the Jupyter python notebook interface on nanoHUB.

Figure 8 shows the GUI of the deployed tool. Users are provided the choice to click “Run” and “Predict using ML” buttons simultaneously or separately depending on the desired information. “Predict using ML” activates the ML surrogate which predicts half of the density profile instantaneously. When a user clicks the “Run” button, the Jupyter notebook passes the selected input parameters to a C++ application to do the preprocessing executed on a virtual machine (VM) allocated by middleware management (Figure 7). Next, the preprocessing script creates the input files required to run the actual MD simulation using the in-house program or LAMMPS [48]. The users are given the option of clicking on “Cluster mode” button for accessing supercomputing resources to lower the computing time. Based on the

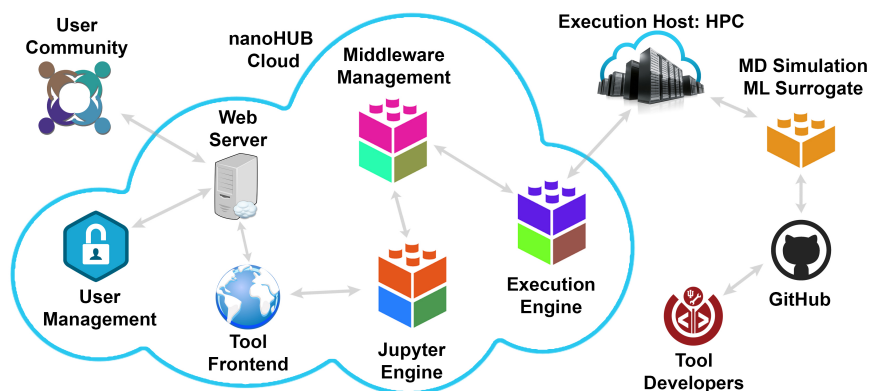


Figure 7: Ecosystem of the computational tool, “Ions in nanoconfinement” [37], deployed on nanoHUB.

state of the “Cluster mode” button, execution engine either submits a job on a computing cluster or runs the simulation on a VM. When the simulation is over, the execution engine passes the generated data to the postprocessing script to generate the positive and negative ion density profiles. These files are plotted on the “Positive Ion Density” and “Negative Ion Density” tabs, and users are provided the option to download the associated data from the “Downloads” tab.

Users can enable ML surrogate any time by clicking the “Predict using ML” button for accessing the ML-predicted ionic density profile. The predicted profile is displayed in the “Prediction Graph” tab. The same prediction graph is also available as an overlay in the “Positive Ion Density” tab when the MD simulation run is completed. ML surrogate is executed inside the Jupyter notebook environment using TensorFlow ML libraries as a separate thread linked to the “Predict using ML” button. For illustration purposes, Figure 8 shows the final density plot using this integrated MD + ML approach for the input parameters $h = 3.0$ nm, $z_p = 1$, $z_n = -1$, $c = 0.5$ M, and $d = 0.714$ nm.

5. Discussion and Conclusion

In this paper, we explored the idea of using scientific ML surrogates to enhance the usability of MD simulations of soft materials for both research and education. The success of the idea was demonstrated using an example soft-matter simulation framework of self-assembling electrolyte ions in nanoconfinement. The overall success rates and rapid inference times associated with the ML predictions enable an interactive, dynamic, and responsive simulation environment open for wide exploration. To facilitate this possibility, we designed and integrated an ML surrogate with the current version of the “Ions in nanoconfinement” computational tool deployed on nanoHUB [37]. The ML-enhanced nanoHUB tool was used to teach nanoscale simulation concepts in an Indiana University course in Fall 2019. As the “Ions in nanoconfinement” framework evolves with more input features (e.g., surface charge density, asymmetric ion sizes) and output quantities, we plan to retrain the ML surrogate to enable predictions for those new input features.

Results from this investigation are encouraging and we intend to explore the feasibility of these ideas in other soft-matter systems including simulations of polymer-based materials which are expected to incur higher computational costs in general. As an example, we plan to explore the design and utility of ML surrogates for MD-based simulated annealing methods used to extract equilibrium shapes of soft-matter-based, deformable nanocontainers [9, 30, 31]. Future work will also explore the extent to which the ML surrogates can predict the desired simulation outputs outside the predefined range of training datasets. The effects of changing the force fields in the MD simulations to propagate the dynamics of ions will be investigated. We also plan to design smart sampling approaches to reduce the amount of training data needed to achieve the desired accuracy associated with the ML surrogate. Finally, we plan to investigate the possibility of extending the idea of an ML surrogate in predicting final outputs to Monte Carlo simulations of materials [42, 24]. We expect that the usefulness of the ML-enabled enhancements demonstrated in this work strengthens the case for scientific simulation applications to be designed and developed with an ML surrogate that learns from the simulations and optimizes the application execution.

ACKNOWLEDGMENTS

This work is supported by the National Science Foundation through Awards 1720625 and DMR-1753182. Simulations were performed using the Big Red II supercomputing system supported in part by Lilly Endowment, Inc., through its support for the IU Pervasive Technology Institute, and in part by the Indiana METACyt Initiative.

Biography

JCS Kadupitiya was born in Sri Lanka in 1990 and completed his Bachelor’s degree in Electrical and Information Engineering from the University of Ruhuna, Sri Lanka, in 2015. He received his Masters in Computer Science and Engineering at the University of Moratuwa, Sri Lanka, in 2017. He also received his second Masters in Computer Engineering from Indiana University Bloomington in 2019, and he is currently enrolled in Indiana University Bloomington as a Ph.D. student in the Department of Intelligent

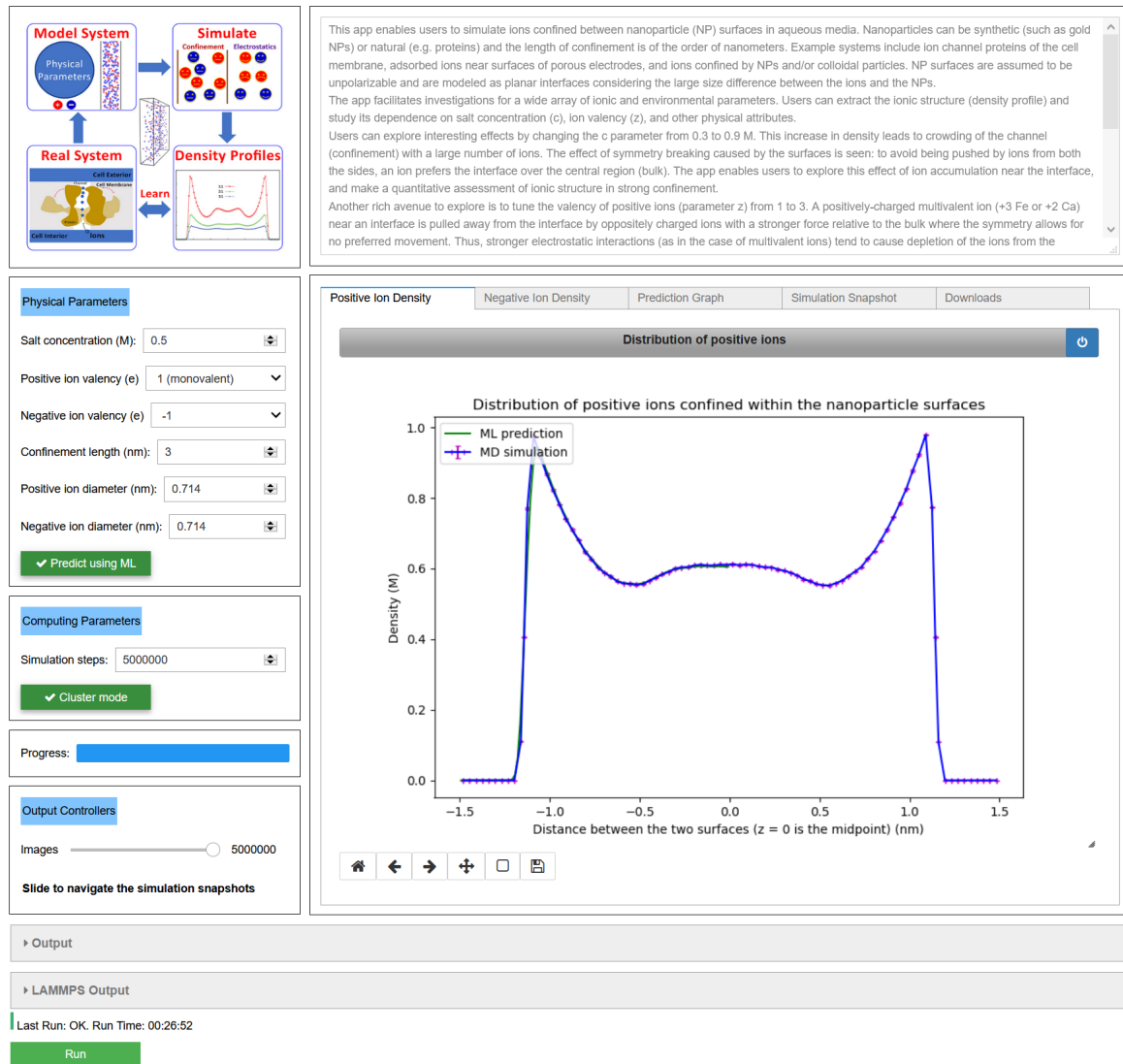


Figure 8: GUI of the ML-surrogate-enhanced “Ions in nanoconfinement” computational tool deployed on nanoHUB [37]. The GUI includes the density profile predicted by the ML surrogate for half of the position values (in green) for an example ionic system. The profile also appears in the “Prediction Graph” tab on the GUI.

Systems Engineering. His research interests lie primarily in scientific machine learning and distributed computing.

Fanbo Sun is a senior undergraduate student at Indiana University majoring in Intelligent Systems Engineering. He is expected to receive his Bachelors degree in 2020. His primary research interests focus on machine learning optimization, deep learning, and natural language processing.

Geoffrey Charles Fox received a Ph.D. in Theoretical Physics from Cambridge University where he was Senior Wrangler. He is now a distinguished professor of Engineering, Computing, and Physics at Indiana University. He previously held positions at Caltech, Syracuse University, and Florida State University after being a postdoc at the Institute for Advanced Study at Princeton, Lawrence Berkeley Laboratory, and Peterhouse College Cambridge. He has supervised the Ph.D. of 73 students with a h-index of 78 and over 36000 citations. He is a Fellow of APS (Physics) and ACM (Computing) and works on the interdisciplinary interface between computing and applications.

Vikram Jadhao is an assistant professor of Intelligent Systems Engineering at Indiana University in Bloomington. Prior to joining Indiana Uni-

versity, he held postdoctoral fellowships in the Department of Physics and Astronomy at Johns Hopkins University as well as the Department of Materials Science and Engineering at Northwestern University. He received his Ph.D. and M.S. in Physics from the University of Illinois at Urbana-Champaign, and his B.S. in Physics from the Indian Institute of Technology at Kharagpur. His current research interests are in nanoscale self-assembly, soft-matter simulation, biomimetic materials, and machine learning. He is a recipient of an NSF CAREER award and an Outstanding Junior Faculty Award from Indiana University Bloomington.

References

- [1] Abadi, M., Barham, P., Chen, J., Chen, Z., Davis, A., Dean, J., Devin, M., Ghemawat, S., Irving, G., Isard, M., et al., 2016. Tensorflow: a system for large-scale machine learning., in: OSDI, pp. 265–283.
- [2] Abruña, H.D., Kiyama, Y., Henderson, J.C., 2008. Batteries and electrochemical capacitors. *Phys. Today* 61, 43–47.
- [3] Allen, R., Hansen, J.P., Melchionna, S., 2001. Electrostatic potential

- inside ionic solutions confined by dielectrics: a variational approach. *Phys. Chem. Chem. Phys.* 3, 4177–4186.
- [4] Barros, K., Sinkovits, D., Luijten, E., 2014. Efficient and accurate simulation of dynamic dielectric objects. *The Journal of Chemical Physics* 140, 064903. doi:10.1063/1.4863451.
- [5] Behler, J., 2016. Perspective: Machine learning potentials for atomistic simulations. *The Journal of chemical physics* 145, 170901.
- [6] Boda, D., Gillespie, D., Nonner, W., Henderson, D., Eisenberg, B., 2004. Computing induced charges in inhomogeneous dielectric media: Application in a monte carlo simulation of complex ionic systems. *Phys. Rev. E* 69, 046702.
- [7] Botu, V., Ramprasad, R., 2015. Adaptive machine learning framework to accelerate ab initio molecular dynamics. *International Journal of Quantum Chemistry* 115, 1074–1083.
- [8] Brunk, N., Kadupitiya, J., Uchida, M., Douglas, T., Jadhao, V., 2019a. Nanoparticle assembly lab. URL: <https://nanohub.org/resources/npassemblylab>, doi:doi:10.21981/RECV-RD32. nanoHUB.
- [9] Brunk, N.E., Jadhao, V., 2019. Computational studies of shape control of charged deformable nanocontainers. *Journal of Materials Chemistry B* 7, 6370. URL: <http://dx.doi.org/10.1039/C9TB01003C>, doi:10.1039/C9TB01003C.
- [10] Brunk, N.E., Uchida, M., Lee, B., Fukuto, M., Yang, L., Douglas, T., Jadhao, V., 2019b. Linker-mediated assembly of virus-like particles into ordered arrays via electrostatic control. *ACS Applied Bio Mat.* 2, 2192–2201. doi:10.1021/acsabm.9b00166.
- [11] Buitinck, L., et al., 2013. Api design for machine learning software: experiences from the scikit-learn project. arXiv:1309.0238 .
- [12] Cawley, G.C., Talbot, N.L., 2010. On over-fitting in model selection and subsequent selection bias in performance evaluation. *Journal of Machine Learning Research* 11, 2079–2107.
- [13] Ch'ng, K., Carrasquilla, J., Melko, R.G., Khatami, E., 2017. Machine learning phases of strongly correlated fermions. *Phys. Rev. X* 7, 031038. doi:10.1103/PhysRevX.7.031038.
- [14] Chollet, F., et al., 2015. Keras.
- [15] Fahrenberger, F., Xu, Z., Holm, C., 2014. Simulation of electric double layers around charged colloids in aqueous solution of variable permittivity. *The Journal of Chemical Physics* 141, 064902. doi:10.1063/1.4892413.
- [16] Ferguson, A.L., 2017. Machine learning and data science in soft materials engineering. *Journal of Physics: Condensed Matter* 30, 043002.
- [17] Glorot, X., Bengio, Y., 2010. Understanding the difficulty of training deep feedforward neural networks, in: *Proceedings of the thirteenth international conference on artificial intelligence and statistics*, pp. 249–256.
- [18] Glotzer, S.C., 2015. Assembly engineering: Materials design for the 21st century (2013 pv danckwerts lecture). *Chemical Engineering Science* 121, 3–9.
- [19] Guo, A.Z., Sevgen, E., Sidky, H., Whitmer, J.K., Hubbell, J.A., de Pablo, J.J., 2018. Adaptive enhanced sampling by force-biasing using neural networks. *The Journal of chemical physics* 148, 134108.
- [20] Hadden, J.A., Perilla, J.R., Schlicksup, C.J., Venkatakrishnan, B., Zlotnick, A., Schulten, K., 2018. All-atom molecular dynamics of the hbv capsid reveals insights into biological function and cryo-em resolution limits. *Elife* 7, e32478.
- [21] Häse, F., Kreisbeck, C., Aspuru-Guzik, A., 2017. Machine learning for quantum dynamics: deep learning of excitation energy transfer properties. *Chemical science* 8, 8419–8426.
- [22] Häse, F., Fdez. Galván, I., Aspuru-Guzik, A., Lindh, R., Vacher, M., 2019. How machine learning can assist the interpretation of ab initio molecular dynamics simulations and conceptual understanding of chemistry. *Chem. Sci.* 10, 2298–2307. URL: <http://dx.doi.org/10.1039/C8SC04516J>, doi:10.1039/C8SC04516J.
- [23] Jadhao, V., 2019. Nanoscale simulations and engineering applications: Applications - self-assembly in nanoconfinement. URL: <https://nanohub.org/resources/29671>.
- [24] Jadhao, V., Makri, N., 2010. Iterative monte carlo path integral with optimal grids from whole-necklace sampling. *The Journal of chemical physics* 133, 114105.
- [25] Jadhao, V., Robbins, M.O., 2017. Probing large viscosities in glass-formers with nonequilibrium simulations. *Proceedings of the National Academy of Sciences* 114, 7952–7957. URL: <https://www.pnas.org/content/114/30/7952>, doi:10.1073/pnas.1705978114.
- [26] Jadhao, V., Robbins, M.O., 2019. Rheological properties of liquids under conditions of elastohydrodynamic lubrication. *Tribology Letters* 67, 66. URL: <https://doi.org/10.1007/s11249-019-1178-3>, doi:10.1007/s11249-019-1178-3.
- [27] Jadhao, V., Solis, F.J., Olvera de la Cruz, M., 2012. Simulation of charged systems in heterogeneous dielectric media via a true energy functional. *Physical review letters* 109, 223905.
- [28] Jadhao, V., Solis, F.J., Olvera de la Cruz, M., 2013a. Free-energy functionals of the electrostatic potential for poisson-boltzmann theory. *Physical Review E* 88, 022305.
- [29] Jadhao, V., Solis, F.J., Olvera de la Cruz, M., 2013b. A variational formulation of electrostatics in a medium with spatially varying dielectric permittivity. *The Journal of chemical physics* 138, 054119.
- [30] Jadhao, V., Thomas, C.K., Olvera de la Cruz, M., 2014. Electrostatics-driven shape transitions in soft shells. *Proceedings of the National Academy of Sciences* 111, 12673–12678.
- [31] Jadhao, V., Yao, Z., Thomas, C.K., Olvera de la Cruz, M., 2015. Coulomb energy of uniformly charged spheroidal shell systems. *Physical Review E* 91, 032305.
- [32] Jing, Y., Jadhao, V., Zwanikken, J.W., Olvera de la Cruz, M., 2015. Ionic structure in liquids confined by dielectric interfaces. *The Journal of chemical physics* 143, 194508.
- [33] Kadupitiya, J.C., Fox, G., Jadhao, V., 2019. Machine learning for auto-tuning of simulation parameters in car-parrinello molecular dynamics, in: *APS Meeting Abstracts*, p. .
- [34] Kadupitiya, J., Brunk, N., Ali, S., Fox, G.C., Jadhao, V., 2018. Nanosphere electrostatics lab. URL: <https://nanohub.org/resources/nselectrostatic>, doi:doi:10.4231/D34X54J88. nanoHUB.
- [35] Kadupitiya, J., Fox, G.C., Jadhao, V., 2019a. Machine learning for parameter auto-tuning in molecular dynamics simulations: Efficient dynamics of ions near polarizable nanoparticles. *IJHPCA Accepted*; arxiv:1910.14620.
- [36] Kadupitiya, J., Fox, G.C., Jadhao, V., 2019b. Machine learning for performance enhancement of molecular dynamics simulations, in: *International Conference on Computational Science*, pp. 116–130. URL: https://link.springer.com/chapter/10.1007/978-3-030-22741-8_9.
- [37] Kadupitiya, K., Anousheh, N., Marru, S., Fox, G.C., Jadhao, V., 2017. Ions in nanoconfinement. URL: <https://nanohub.org/resources/nanoconfinement>, doi:doi:10.21981/D236-ZZ44. nanoHUB.
- [38] Kasim, M., Watson-Parris, D., Deaconu, L., Oliver, S., Hatfield, P., Froula, D., Gregori, G., Jarvis, M., Khatriwala, S., Korenaga, J., et al., 2020. Up to two billion times acceleration of scientific simulations with deep neural architecture search. arXiv preprint arXiv:2001.08055 .
- [39] Klimeck, G., McLennan, M., Brophy, S.P., III, G.B.A., Lundstrom, M.S., 2008. nanohub.org: Advancing education and research in nanotechnology. *Computing in Science Engineering* 10, 17–23.
- [40] Kremer, K., Grest, G.S., 1990. Dynamics of entangled linear polymer melts: A molecular-dynamics simulation. *J. Chem. Phys.* 92, 5057–5086.
- [41] Limbach, H.J., Arnold, A., Mann, B.A., Holm, C., 2006. ESPResSo – an extensible simulation package for research on soft matter systems. *Comp. Phys. Comm.* 174, 704–727.
- [42] Liu, J., Qi, Y., Meng, Z.Y., Fu, L., 2017. Self-learning monte carlo method. *Phys. Rev. B* 95, 041101.
- [43] Long, A.W., Zhang, J., Granick, S., Ferguson, A.L., 2015. Machine learning assembly landscapes from particle tracking data. *Soft Matter* 11, 8141–8153.
- [44] Luo, G., Malkova, S., Yoon, J., Schultz, D.G., Lin, B., Meron, M., Benjamin, I., Vanýsek, P., Schlossman, M.L., 2006. Ion distributions near a liquid-liquid interface. *Science* 311, 216–218.
- [45] Morningstar, A., Melko, R.G., 2017. Deep learning the ising model near criticality. arXiv preprint arXiv:1708.04622 .

- [46] Nygård, K., Sarman, S., Kjellander, R., 2013. Local order variations in confined hard-sphere fluids. *The Journal of Chemical Physics* 139, 164701.
- [47] Perilla, J., Hadden, J., Goh, B., Mayne, C., Schulten, K., 2016. All-atom molecular dynamics of virus capsids as drug targets. *The journal of physical chemistry letters* 7, 1836–1844. URL: <https://pubs.acs.org/doi/10.1021/acs.jpcllett.6b00517>.
- [48] Plimpton, S., 1995. Fast parallel algorithms for short-range molecular dynamics. *Journal of Computational Physics* 117, 1 – 19.
- [49] Schoenholz, S.S., 2018. Combining machine learning and physics to understand glassy systems. *Journal of Physics: Conference Series* 1036, 012021.
- [50] Smith, A.M., Lee, A.A., Perkin, S., 2016. The electrostatic screening length in concentrated electrolytes increases with concentration. *The journal of physical chemistry letters* 7, 2157–2163.
- [51] Solis, F.J., Jadhao, V., Olvera de la Cruz, M., 2013. Generating true minima in constrained variational formulations via modified lagrange multipliers. *Physical Review E* 88, 053306.
- [52] Spellings, M., Glotzer, S.C., 2018. Machine learning for crystal identification and discovery. *AIChE Journal* 64, 2198–2206.
- [53] Wang, J., Olsson, S., Wehmeyer, C., Perez, A., Charron, N.E., De Fabritiis, G., Noe, F., Clementi, C., 2019. Machine learning of coarse-grained molecular dynamics force fields. *ACS central science* .